Bifurcating, chaotic, and intermittent solutions in the rf-biased Josephson junction

Miguel Octavio
Fundación Instituto de Ingeniería e Instituto Venezolano de Investigaciones Científicas, Apartado 40200, Caracas 1040A, Venezuela
(Received 11 August 1983)

Extensive numerical simulations of the rf-biased Josephson junction are presented. It is shown that, as the amplitude is increased for fixed damping and frequency, an apparently endless sequence of bifurcating-chaotic trees separated by periodic solutions exists. The state diagram characterized in the amplitude-damping plane at fixed frequency ($\Omega=0.65$) shows a complex set of solutions. A detailed study of the transition in the high-damping limit is presented, indicating the bounds for asymmetric, bifurcating, and chaotic solutions for low β_c. It is shown that strange attractors are common to trapped and free-running chaotic solutions for nearby amplitudes due to intermittency among the various basins of attraction. Return maps at high amplitudes are found to be essentially one dimensional. Experimental consequences of our simulations are presented in terms of equivalent noise temperatures at low frequencies, resulting in maximum noise temperatures of the order of 10^6–10^7 K.

I. INTRODUCTION

The existence of chaotic solutions and the transition to chaos in dissipative dynamical systems have generated wide interest in the past few years[1] due in part to a number of universalities that are found both in irreversible maps and in a wide variety of nonlinear differential equations. One such nonlinear dynamic system is the driven Josephson junction, a system isomorphic to a variety of physical systems such as the driven damped pendulum, a particle in a driven periodic potential or a charge density wave pinned to its lattice.[2] Interest in the chaotic behavior of Josephson junctions was initially generated by the suggestion of Huberman *et al.*[3] that chaotic solutions might be responsible for the observed large noise rise in Josephson junction parametric amplifiers,[4–6] as well as calculations by Kautz,[7,8] showing the existence of universalities like those of one-dimensional noninvertible maps[9] in the presence of a dc bias. Further simulations by Pederson and Davidson[10] revealed a rather complex state diagram in the amplitude-frequency plane with structure not previously observed in analog simulations[3] for rf-driven junctions. D'Humieres *et al.*[11] showed a variety of significant features associated with chaotic solutions in rf-driven junctions, such as the importance of symmetry breaking, low-frequency chaotic solutions, and the role of intermittency between phase-locked states. In fact, simulations have shown intermittency to be quite generic to a variety of Josephson junction circuits both in the rf-bias[12] and dc-bias[13] cases, and has been observed in real junctions in a resonant circuit by Miracky *et al.*[14] Experimental understanding of chaos in the rf-driven junction still remains unclear. Parametric amplifiers that have shown unusually large noise rises[4–6] include those made with junctions with low capacitances where chaotic solutions are not expected to occur. Furthermore, Levinson[15] has shown, using analog simulations, that no chaotic solution exists at the operating points where parametric amplification occurs.

The rf-driven junction is the simplest system in which one can hope to compare the experimental behavior of real junctions to simulations, since it contains the fewest experimental parameters of those Josephson junction systems that have been found to exhibit chaotic solutions. Such a comparison should not only provide information about the transition to chaos and the chaotic state in Josephson junctions, but might also yield information about the adequacy of models of Josephson junctions.

In this paper extensive simulations that complement previous simulations for the rf-driven Josephson junction are presented. Owing to the interest in the transition to the high-damping regime, a state diagram has been calculated in the rf amplitude-damping plane at a fixed frequency up to amplitudes higher than those previously studied. It is shown that as the rf amplitude increases, the solutions show a sequence of period-doubling cascades into a complex chaotic-intermittent state. While each region in the sequence varies in detail from the others, they are all qualitatively similar to the period-doubling-chaotic cascade in one-dimensional maps. Each region contains phase-locked and unlocked solutions and is followed by a transition into period-one solutions either directly from a chaotic state or through a period-two sequence. Intermittent regions are found in the transition to odd-period bifurcations, with features similar to tangent bifurcations, but the detailed behavior is more complicated than that of one-dimensional maps. The detailed transition in the high-damping regime shows a period-two region that becomes chaotic as the damping is reduced. The bounds for this behavior are lower than the characteristics damping value of the hysteretic I-V characteristics of Stewart and McCumber[16] for a dc-biased junction. Noise temperatures show that in the absence of thermal fluctuations an upper limit of $\sim 3\times 10^6$ K exists for a 1-mA junction. The effect of thermal fluctuations is also discussed.

The organization of the paper is as follows. In Sec. II

the equations for the rf-driven junction are presented together with a discussion of the simulation techniques used. In Sec. III we discuss a typical sequence with increasing rf drive at fixed frequency and damping. In Sec. IV the state diagram at fixed frequency is presented and the high-damping limit is discussed. In Sec. V we discuss strange attractors, intermittency, and return maps associated with the state diagram of Sec. IV. Finally, in Sec. VI we discuss applications of our simulations to experiments and in Sec. VII we present our conclusions.

II. THE RESISTIVELY SHUNTED JUNCTION MODEL

The rf-driven Josephson junction is modeled using the usual shunted junction model, which assumes that the junction is effectively current-biased by an rf drive. Then if a Josephson element is shunted by a fixed resistance R_N and a capacitor C we can write

$$C\frac{dV}{dt}+\frac{V}{R_N}+I_C\sin\phi=I_{\rm rf}\sin(\omega t)\ , \tag{1}$$

where ϕ is the total phase difference across the junction and $I_{\rm rf}$ is the rf current.

This equation combined with the second Josephson relation

$$\hbar\frac{d\phi}{dt}=2eV \tag{2}$$

can be reduced to a single dimensionless third-order equation

$$\frac{d^2\phi}{dt^2}+\frac{1}{\sqrt{\beta_c}}\frac{d\phi}{dt}+\sin\phi=\rho\sin(\Omega t)\ , \tag{3}$$

where time has been normalized by the inverse of the plasma frequency $\omega_p=(2eI_c/\hbar C)^{1/2}$, the natural frequency of the system, ρ is the rf-driving amplitude $I_{\rm rf}$ normalized by the critical current I_c, Ω is the normalized applied frequency, and β_c is the Stewart-McCumber parameter $\beta_c=2eI_cR_N^2C/\hbar$, which is a measure of the damping of the system.

As noted in the Introduction, Eq. (3) is isomorphic to the driven damped pendulum,[11] charge-density waves in the presence of time-varying electric field, and a charged particle in a viscous medium in a sinusoidal potential with a time-varying electric field. In what follows we will use the latter analog in order to understand qualitatively some features of the solutions to Eq. (3).

Solutions to Eq. (3) were obtained using a fourth-order Runge-Kutta algorithm. After transients died out, a search was made for solutions of the form $\phi(t+(2\pi/\Omega)l)=\phi(t)+2\pi nl$ and $\dot\phi(t+(2\pi/\Omega)l)=\dot\phi(t)$, where n and l are integers. Typically, both initial conditions were set to zero, which yields both stable and unstable solutions. In order to study the effect of noise on regimes of the parameter space and to eliminate unstable solutions, noise was introduced in our calculations.

In the presence of thermal fluctuations and as long as $eV\gg k_BT$, the autocorrelation of the noise current is given by the usual Johnson noise expression

$$\langle I_n(t)I_n(t+\tau)\rangle=(2k_BT/R_N)\delta(\tau)\ . \tag{4}$$

Since a Gaussian distribution with a finite width is used to generate noise events, the normalized noise current $\rho_n=I_n/I_c$ autocorrelation is then given by

$$\langle\rho_n(t)\rho_n(t+\tau)\rangle=(4/\gamma\beta_c^{1/2}\Delta t)\delta(\tau)\ , \tag{5}$$

where Δt is the normalized time step used in the calculation and $\gamma=\hbar I_c/ek_BT$ is the noise parameter of Ambegaokar and Halperin.[17]

Using (5) and (3), one can then write the usual Langevin equation for the Josephson junction in the presence of noise. In general, a time step Δt between 0.01 and 0.001 was used and typical transients were found to be of the order of 30–50 driving force periods. In the case of tangentlike bifurcations, even a larger number of periods had to be neglected to guarantee the attainment of a steady state. When needed, the power spectrum of the voltage was calculated using

$$S_{\dot\phi}(\Omega)=\frac{2}{T}\left|\int_0^T\dot\phi(\tau)e^{i\Omega t}dt\right|^2\ , \tag{6}$$

with averaging times of up to 512 periods of the rf drive.

III. SOLUTIONS WITH INCREASING rf DRIVE

Figure 1(a) shows a qualitative representation of the types of solutions observed as the amplitude of the rf drive is increased from $\rho=0.8$ to $\rho=10$ for fixed damping ($\beta_c=5$) and normalized frequency ($\Omega=0.65$). This value of the normalized frequency was chosen since we found the richest structure in the state diagram around this particular value. Triangular regions indicate qualitatively whether subharmonic or chaotic solutions are observed. A total of eight regions are shown in Fig. 1(a). For the particular damping represented in Fig. 1(a), each of the eight regions begins with a period doubling sequence followed by chaotic solutions. Within each chaotic region, a variety of phenomena are found, the most common feature being the existence of period-three and -five windows. Figure 1(b) shows the average voltage across the junction for each region in Fig. 1(a). [To generate Fig. 1(b), we introduced a small amount of noise corresponding to 0.5 K for a junction with a 1-mA critical current in order to eliminate unstable solutions. Similarly, the rf bias was increased smoothly in order to have symmetry breaking of the same sign, which does not occur for a fixed set of initial conditions at each rf drive.] In general, the average voltage of any period-two solutions corresponds to a phase-locked solution. Within the chaotic regime, it is possible to observe both phase-locked and unlocked solutions, the former commonly following or preceding regions of subharmonic or period-one behavior.

There are two significant features in Fig. 1. First, as the amplitude increases, there is an apparently endless sequence of bifurcating-chaotic trees. Second, phase-locked solutions on a step other than the $n=0$ are only present at low rf drives. The origin of the sequence of bifurcating-chaotic trees can be understood by considering the analog of a forced charged particle moving in a sinusoidal potential. As pointed out by D'Humieres *et al.*,[11] the signature preceding the bifurcating cascade is the onset of symmetry breaking. Symmetry breaking begins as the particle starts

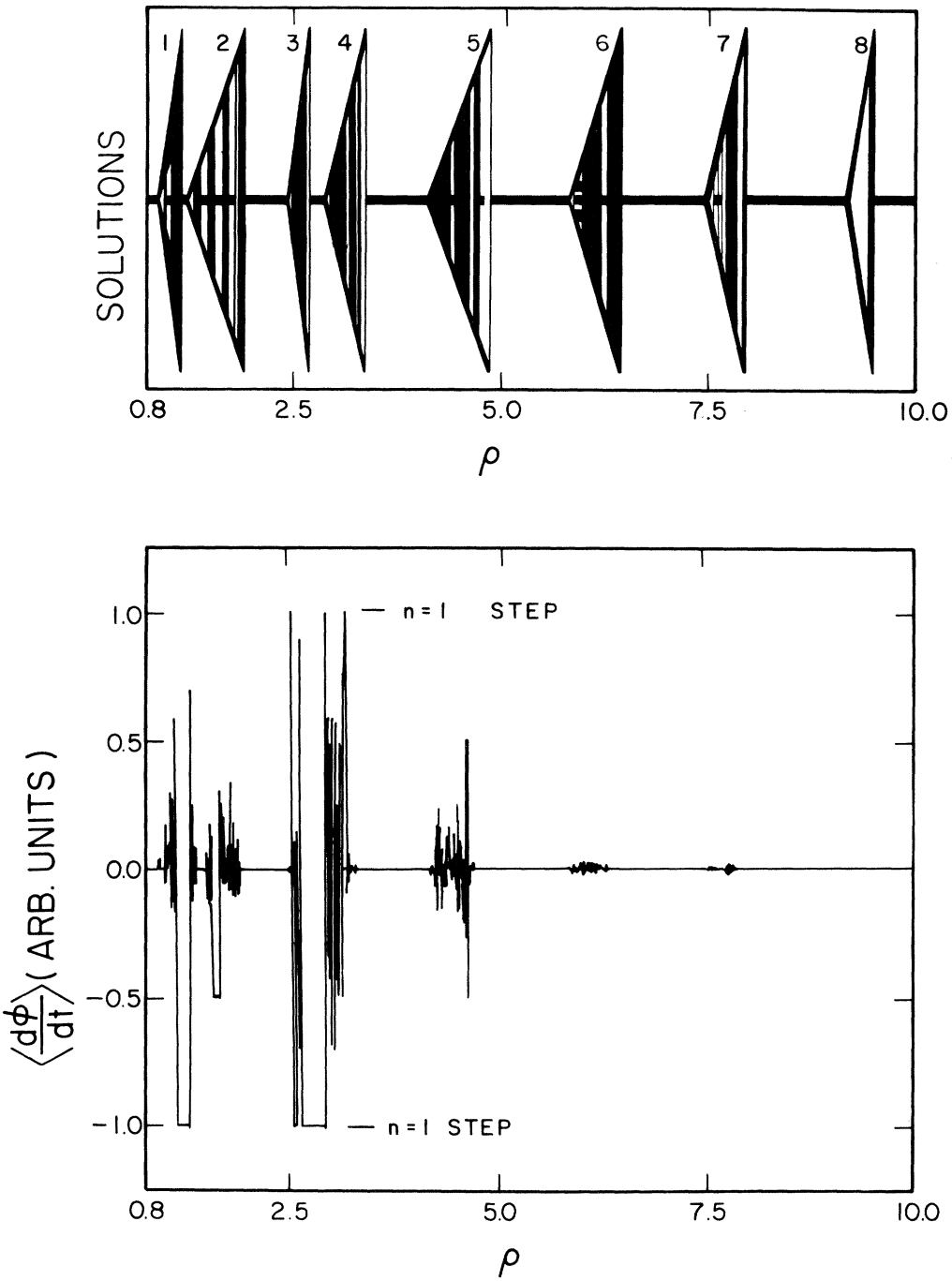

FIG. 1. (a) Schematic representation of the type of solutions found for $\Omega=0.65$ and $\beta_c=5$ as a function of the rf amplitude ρ. For any given ρ, the character of the solution is represented by one point (period one), two points (period 2^k), three points (3×2^k), five points (period 5×2^k), or solid (chaotic solutions). All higher-order solutions are not indicated and only major regions are indicated. (b) Average voltage $\langle d\phi/dT\rangle$ of solutions for the same parameters as used in (a). Note how phase-locked solutions on the $n=1$ step and subharmonic steps are absent at high amplitudes. Note also how the fluctuations in voltage become smaller as the amplitude is increased.

to "explore" the nonlinear part of the first well in which its motion began. (In the driven damped pendulum, this corresponds to larger oscillations around the equilibrium position.) At slightly higher amplitudes, the period-doubling sequence develops, followed by the chaotic regime, which begins to occur as the particle moves near a maximum in the sinusoidal potential. The motion of the particle becomes periodic again as the slow motion of the particle occurs near the minima of the first well (where the oscillations began at low amplitude) and near the minima of the adjacent well. If the rf drive is increased further, the motion repeats the same qualitative sequence. The symmetry is broken again as the particle excursion reaches the nonlinear part of each of the two neighboring

wells. This is followed by another bifurcation tree and chaos as the rf amplitude is increased. Thus, the series of chaotic trees corresponds to essentially the same motion, except that the particle visits an additional well for each region. Thus, one would expect an endless sequence of bifurcating-chaotic regions as motion in each additional well generates an additional bifurcating-chaotic sequence.

The simple picture described above is complicated by the existence of periodic-running solutions. These occur whenever "strong" asymmetry is observed and the motion of the particle reaches an additional well on one side. An example of this behavior for the first region of Fig. 1(a) at low rf drive is shown in Fig. 2. Figure 2(a) shows the phase-plane solution at the beginning of the first bifurcating sequence together with the real motion in the sinusoidal potential. Figure 2(b) shows the phase-plane solution for the second region of Fig. 1(a). There is strong symmetry breaking, which results in a free-running solution, as shown in the inset in Fig. 2. Thus, regions 1 and 2 of Fig. 1(a) correspond to oscillations within one well, the difference being that the second is a free-running solution (phase locked or not) in which in each cycle the particle oscillates once in each well and diffuses to the next one, thus yielding a nonzero average voltage. This solution is phase locked and corresponds to the $n=1$ step of Fig. 1(b).

The eight ($\beta_c=5$) regions in Fig. 1(a) thus correspond to oscillations in the first six wells, with the second and fourth regions corresponding to free-running solutions with strong symmetry breaking.

It is difficult to determine the space variables required for strong symmetry breaking. In general at very high rf drives no free-running solutions are observed, which is somewhat counterintuitive. Figure 3 shows the motion in the initial bifurcating regime corresponding to motion in the first five wells (or first five rotations of the pendulum), clearly indicating the origin of the series of sequences described earlier.

For all regions studied, it is clear that *the slow motion of the cycle is critical in determining the subsequent behavior.* Symmetry breaking begins when slow motion occurs near the nonlinear part of the well, chaotic solutions begin to occur as the slow motion gets close to the maxima of the potential, and period-one solutions reappear when the slow motion reaches the minima of the adjacent wells.

Careful study of symmetry breaking shows that the direction of asymmetry depends on which side of the well the nonlinear regime is first visited. This is strongly dependent on the initial conditions.

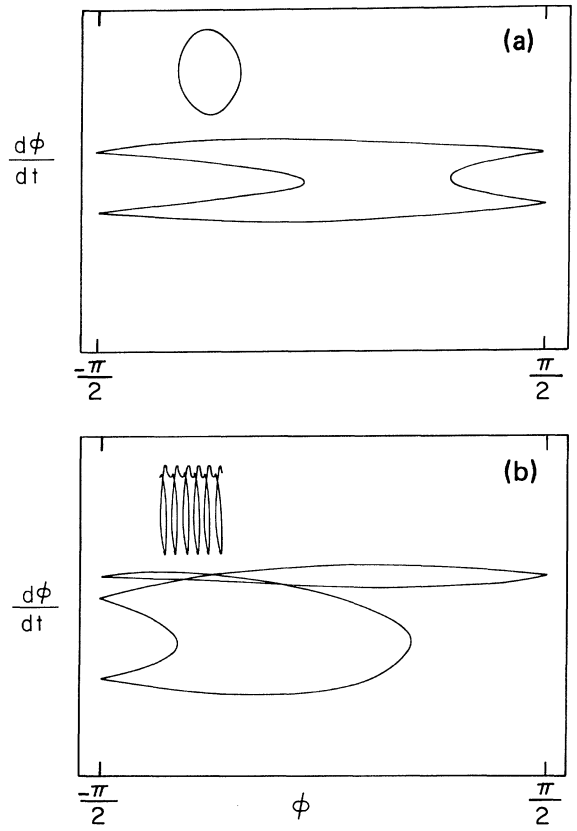

FIG. 2. (a) Phase-plane solution $\dot{\phi}$ vs ϕ (mod π) for a periodic solution with broken symmetry near the first bifurcating-chaotic region ($\beta_c=5$, $\Omega=0.65$, $\rho=0.925$). The inset shows the solution $\dot{\phi}$ vs ϕ in "real" space showing the single-well "trapped" motion. (b) Phase-plane solution $\dot{\phi}$ vs ϕ for strong symmetry breaking near the second bifurcating-chaotic region. The inset demonstrates the free-running nature of the solution ($\beta_c=5$, $\Omega=0.65$, $\rho=1.25$). Both insets are in arbitrary units.

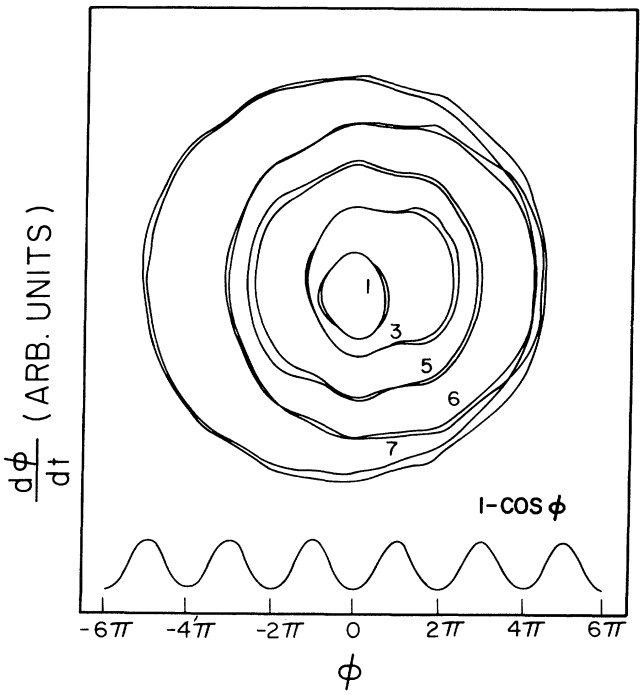

FIG. 3. Phase-plane solutions $\dot{\phi}$ vs ϕ in "real" space showing the bifurcating solutions at the beginning of the regions 1, 3, 5, 6, and 7 of Fig. 1, which show trapped solutions. The bottom shows the sinusoidal potential. Clearly, each succesive region corresponds to adding an additional well to the motion. All trajectories are for $\beta_c=5$ and $\Omega=0.65$. Amplitudes are for each region $\rho_1=0.95$, $\rho_3=2.51$, $\rho_5=4.185$, $\rho_6=5.85$, and $\rho_7=7.52$. Note the effect on the limit cycle velocity due to the potential.

IV. THE STATE DIAGRAM

A. General features

While extensive characterization of solutions has been made in the amplitude-frequency plane with fixed damping,[3,10,11,18] it is of interest to consider the amplitude-damping state diagram at fixed frequency. This interest is twofold: first, it allows for the study of the transition to the high-damping regime; second, it is a useful guide in considering possible experiments with real junctions where it should be possible to vary β_c by varying temperature, and thus "tune" the junction to regions where a rich variety of solutions can be observed.

Figure 4 shows the state diagram in the rf amplitude-damping plane up to $\beta_c=25$ for a fixed frequency near the plasma frequency ($\Omega=0.65$). This diagram was generated in the absence of noise starting from zero initial conditions. The state diagram of Fig. 4 shows in detail the solutions obtained at low rf excitation amplitudes ρ. The dark regions represent subharmonic solutions of the form $2^K\times n$, where n is indicated in the figure and $K=1,2,3,\ldots$. The dashed regions indicate chaotic solutions, and the empty regions indicate period-one solutions. For clarity, only major subharmonic regions with $n=2$, 3, and 5 are indicated. Similarly, no indication is given as to whether the solution is phase locked or not. The state diagram in Fig. 4 is only modified slightly by the addition of small noise temperature. Unstable solutions typically correspond to small regions of subharmonic behavior or to regions of oscillations around the potential maxima (or the up position in the pendulum analogy).

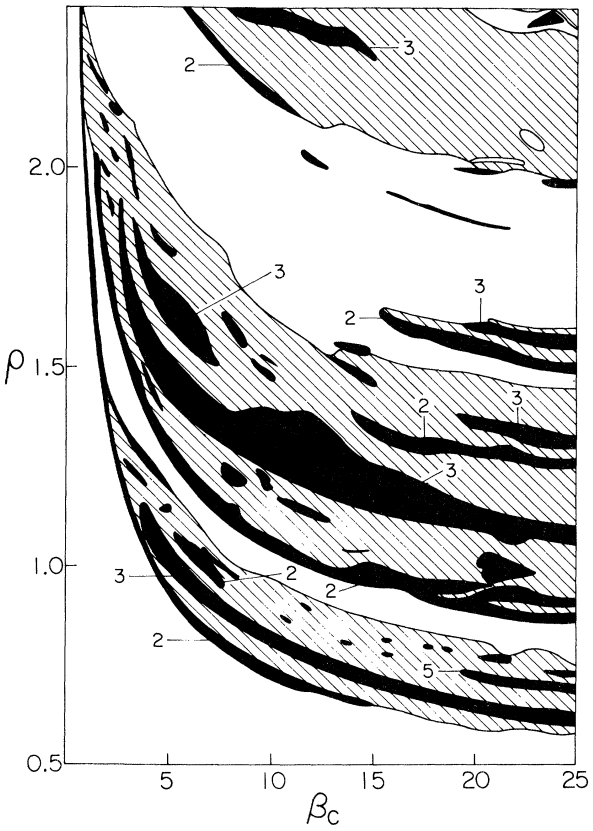

FIG. 4. State diagram in the amplitude-damping plane for $\Omega=0.65$ showing the different periodicity of the solutions. Empty regions correspond to period-one solutions. Solid regions correspond to period doubling, tripling, and quintupling, as indicated in the figure. Cross-hatched regions indicate chaotic solutions. Only major bifurcating-chaotic solutions are indicated. The diagram was generate by exploring the solution plane with a grid $\Delta\rho=0.01$ and $\Delta\beta_c=0.025$ starting from zero initial conditions in the absence of noise.

While complex, the map shown in Fig. 4 shows the finer structure of each of the series of regions discussed in Sec. III. Each period-one region is followed by a bifurcating cascade of the form 2^k, which in turn leads to chaotic solutions (dashed regions). The cascade always follows Feingenbaum's scenario within the numerical precision used. However, we have found incomplete cascades in which the cascade reverses itself without reaching a chaotic regime. In analogy with irreversible maps, period-three and -five regions are found within the chaotic regime. Period-three regions are usually the widest observed. Higher-order regions tend to be narrow and are more commonly observed for high β_c values.

It is interesting to consider the motion in the period tripling regions, as shown in Fig. 5 for $\rho=1.025$. The figure shows the phase-space plot, and the inset shows the motion in real space for a particle in a sinusoidal well. Once again, the slow motion part of the cycle appears to be crucial. The particle makes two small symmetric oscillations within the first well after which it travels symmetrically to the two adjacent wells. Each small oscillation takes one period of the driving frequency, and the motion in the adjacent wells takes another period. As the amplitude is increased, the small oscillations begin to occur closer and closer to the maxima until the period tripling breaks down near the maxima and chaotic behavior is restored.

Period-one and subharmonic regions are always phase locked, and it is possible to switch from a phase-locked $n=1$ solution to an $n=2$ solution, a behavior observed,

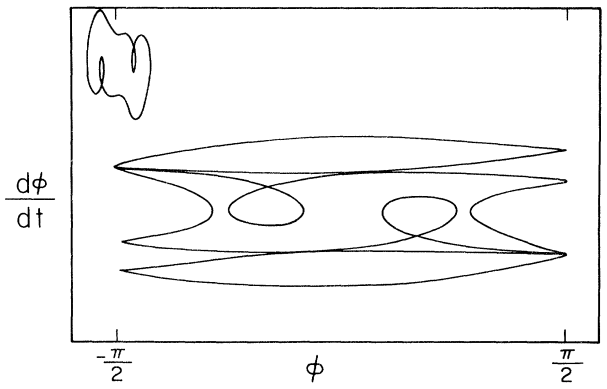

FIG. 5. Phase-plane solution $\dot{\phi}$ vs ϕ (mod π) for a typical tripling region ($\Omega=0.65$, $\beta_c=5$, $\rho=1.025$). Amplitude changes simply change the location and size of the two antisymmetric loops. The inset has arbitrary units.

for example, in the wide period-one region near $\rho=2$ for β_c values larger than 10. For $\beta_c=25$ the state diagram of Fig. 4 agrees quantitatively with the solutions of Pedersen and Davidson.[10] On the other hand, the map agrees with that of D'Humieres *et al.*[11] only qualitatively, the details of the observed sequence are the same, but the rf amplitudes at which the sequences begin are much higher in the calculated state diagram. In contrast to the analog simulations of Cirillo and Pedersen,[18] the transition to chaos for $\beta_c<15$ occurs through a bifurcating tree.

The overall effect on the ρ-β_c state diagram of varying the frequency of the rf drive can be summarized as follows: As the frequency is lowered below $\Omega=0.65$ each bifurcating-chaotic region becomes narrower and the spacing between regions is reduced. At sufficiently low frequencies all regions merge, leaving only wide chaotic zones. Simultaneously the range of β_c values for which the initial transition to chaos occurs without bifurcations increases in size, bifurcating cascades occurring only at the lowest β_c values. For larger Ω values (but $\Omega\leq 1$) the opposite is observed. This indicates that in any experiment with real junctions, there is an optimum range between $0.65\leq\Omega\leq 1$ where a rich variety of solutions occur over the widest amplitude range. In this frequency interval, transitions to chaos occur through bifurcating cascades over the widest damping range.

B. Transition to the high-damping limit

The transition to the high-damping limit ($\beta_c\rightarrow 0$) is of interest for a variety of reasons. First, this limit corresponds to a second-order nonlinear differential equation for which no bifurcations or chaotic solutions are expected. Second, the experimental evidence[4] that initially generated interest in the chaotic behavior of Josephson junctions came from parametric amplifiers that used low β_c superconducting microbridges as the nonlinear element. Finally, it is intriguing to explore whether such transitions exhibit critical behavior. Figure 6 shows in detail the region of low β_c of the state diagram shown earlier, displaying the bounds for asymmetric, bifurcating, and chaotic solutions. For $\beta_c\lesssim 0.04$ all solutions are symmetric and periodic at this frequency. Above $\beta_c\cong 0.04$, solutions exhibit symmetry breaking up to $\beta_c=0.632$, where incomplete 2^k cascades emerge. With increasing rf amplitude at fixed β_c the bifurcating reverses itself before solutions once again become periodic. For higher β_c values, both the forward and reverse cascades develop fully and are separated simultaneously by regions of chaotic solutions. The appearance of the reverse cascade, while not a common feature of one-dimensional maps, is often observed in rf-biased Josephson junctions.[11] For example, in Fig. 1, regions 3–5 exhibit this reverse sequence. It is clear from Fig. 6 that both pitchfork bifurcations and chaotic solutions can occur even in nonhysteretic junctions. The onset of chaotic solutions occurs at $\beta_c=0.788$, which is below the Stewart-McCumber[16] value for hysteretic junctions. Figure 7 shows a sequence of phase-space portraits for fixed amplitude and increasing β_c showing typical solutions found for the state diagram shown in Fig. 6.

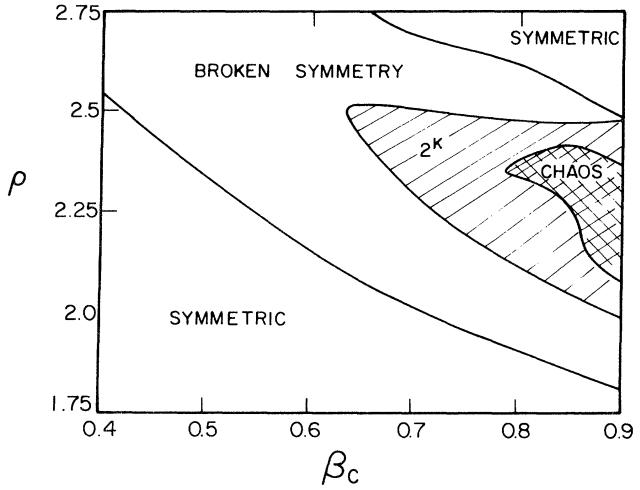

FIG. 6. State-diagram ρ-β_c in the low β_c regime showing the bounds for observation of asymmetric, bifurcating, and chaotic solutions. The hatched region shows bifurcating 2^k solutions that can reverse-flip as the amplitude is increased at fixed β_c. The 2^k sequence is also found to be truncated for β_c values for which no chaotic solutions exist ($\Omega=0.65$).

The low β_c transition shown in Fig. 6 clearly demonstrates that low capacitance microbridges are unlikely to exhibit large noise rises as noted by Levenson and Feldman.[19] This, of course, presupposes that a microbridge can be described adequately by Eq. (1) where any possible inductive, heating,[20] or nonequilibrium effects have been neglected. Thus, while the results of Chiao *et al.*[4] originally motived much of the interest in chaos in Josephson junctions, no simulation has yet provided a clear-cut explanation of their experimental observation.

As β_c decreased below 10, the minimum amplitude $\rho_{\min}$ for which bifurcations are observed increases smoothly down to $\beta_{c\,\min}=0.6$ but no phase-transition-like relationship of the form $\rho_{\min}\propto 1/(\beta_c-\beta_{c\,\min})^{\alpha}$ is observed. It is found that each of the first four bifurcating regions for low β_c at $\Omega=0.65$ can be parametrized rather well by $\rho_{\min,j}=\gamma_j/\beta_c\alpha_j$, where γ is a constant for each of the j regions and $\alpha_1=0.445\pm 0.002$, $\alpha_2=\alpha_3=0.317\pm 0.002$, and $\alpha_4=0.197\pm 0.002\cong\alpha_1^2$. While the exact exponents change with Ω, the relationships between exponents remain valid for three points calculated between $\Omega=0.65$ and 0.78.

V. STRANGE ATTRACTORS, RETURN MAPS, AND INTERMITTENCY

The strange attractor corresponding to the first bifurcating-chaotic region of Fig. 1(a) is shown in Fig. 8, together with its power spectrum $S_{\dot\phi}(\Omega)$. The regions occupied by the 2^k and 3×2^k attractors are also indicated. While the value of the rf amplitude corresponds to the first region of Fig. 1(a), the same strange attractor is observed for the second region, which is characterized by free-running solutions with one oscillation per well. Figure 9 shows in detail how in a manner analogous to one-dimensional irreversible maps,[21,22] the section of the 3×2^k attractor, shows intermittency, as the period tripling re-

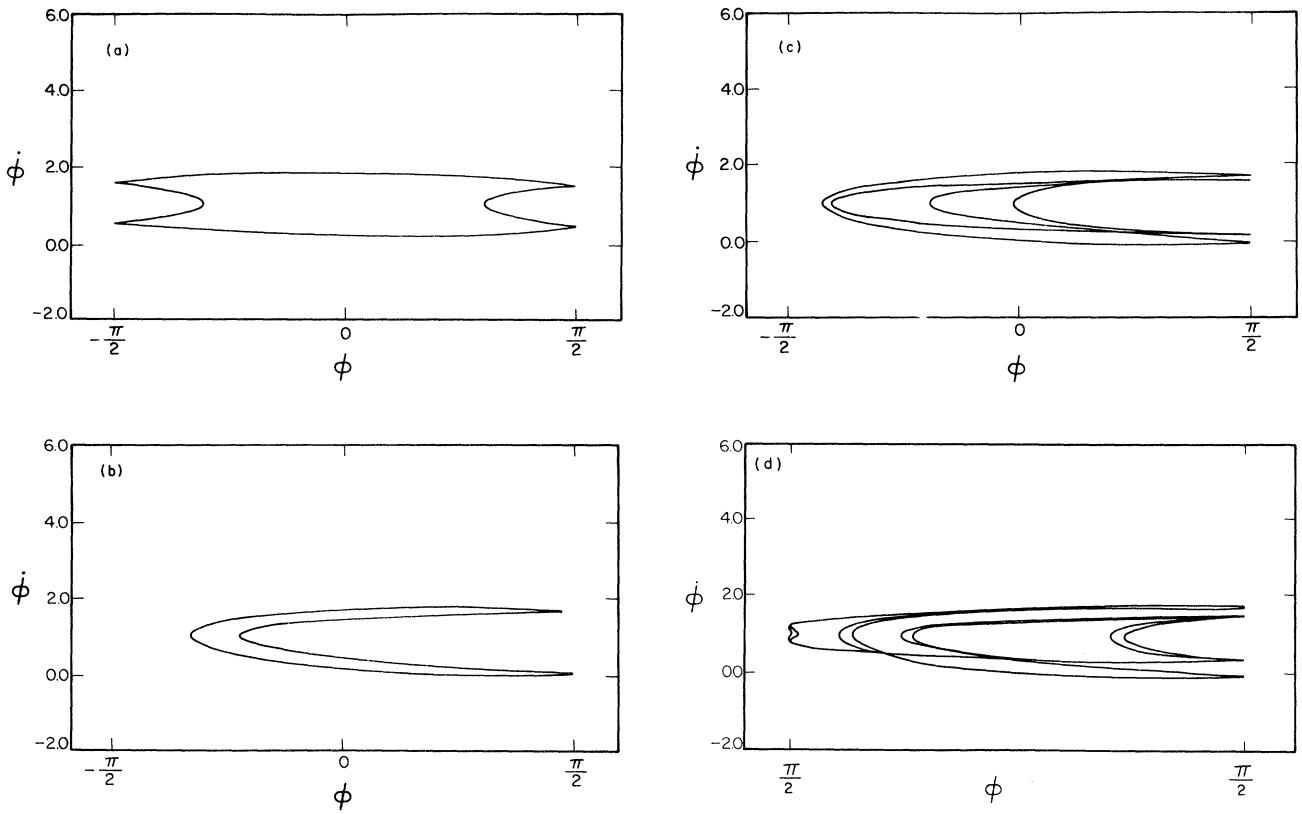

FIG. 7. Typical sequence of phase-plane portraits $\dot{\phi}$ vs ϕ for fixed amplitude ($\rho=2.35$) and increasing β_c showing the strong changes in solutions: (a) total symmetry ($\beta_c=0.4$), (b) broken symmetry ($\beta_c=0.64$), (c) period doubling ($\beta_c=0.72$), and (d) period four ($\beta_c=0.78$).

gion is approached. Note that this basin of attraction is common to both 3×2^k regions found for single-well (region 1) and free-running (region 2) solutions. As the amplitude is increased, the 3×2^k cascade develops, and once past the tripling window the same attractor shown in Fig. 8 reappears. The strange attractor of Fig. 8 is found to be a composite of the attractors corresponding to harmonic and subharmonic chaotic phase-locked states found in the first two regions described in Sec. III. Thus, the numerical simulations exhibit the same type of intermittent behavior noted by D'Humieres *et al.*[11] using analog simulations. Since in our case the solutions are computed in the absence of noise, it is clear that this intermittency is an intrinsic property of the motion and is not due to possible noise-induced transition between chaotic phase-locked states. The observed Poincaré maps may contain more than two attractors, hence, the behavior is reminiscent of the model proposed by Ben-Jacob *et al.*,[13] in which only two attractors are involved in the motion.

Figure 10 displays the first five strange attractors. At higher amplitudes their structure seems to be much simpler, a consequence of the absence of intermittent-chaotic solutions, since past the fourth of the regions in the sequence, only the $n=0$ phase-locked state is observed. The complexity of the calculated solutions would suggest that any attempt to construct a return map for either ϕ and $\dot{\phi}$ would be quite difficult since the Poincaré maps imply that a two-dimensional return map is required. In fact, we find that intermittency between almost-stable phase-locked states is the most significant obstacle. This is demonstrated in Fig. 11, which shows calculated return maps for three regions, one [Fig. 11(a)] with intermittent-chaotic behavior and two in which this phenomena is absent [Figs. 11(b) and 11(c)]. In Fig. 11(a) the nature of the map is quite difficult to discern. Note in particular the presence of dense regions of "random" points near $\phi=0$ and 2π. In contrast to Fig. 11(a), at higher amplitudes the return maps become well-behaved functions on the interval with no "random" points. As the amplitude is increased the return maps [Figs. 11(b) and 11(c)] become simpler and show features quite similar to one-dimensional maps such as the logistic equation. The dense regions near $\phi=0$ and 2π in Fig. 11(a) reflect the hopping between basins of attraction, which introduces an additional random contribution to the already quasiperiodic motion of the chaotic state. This motion between attractors is not contained in the Ben-Jacob *et al.*[13] model where the motion is assumed to switch between nearby attractors, but the details of the transient motion are neglected.

A different type of intermittency for one-dimensional maps has been described by Manneville and Pomeau[21] and Hirsh *et al.*,[22] and studied in Josephson junctions by Yeh and Kao[12] using analog simulations. This intermittent

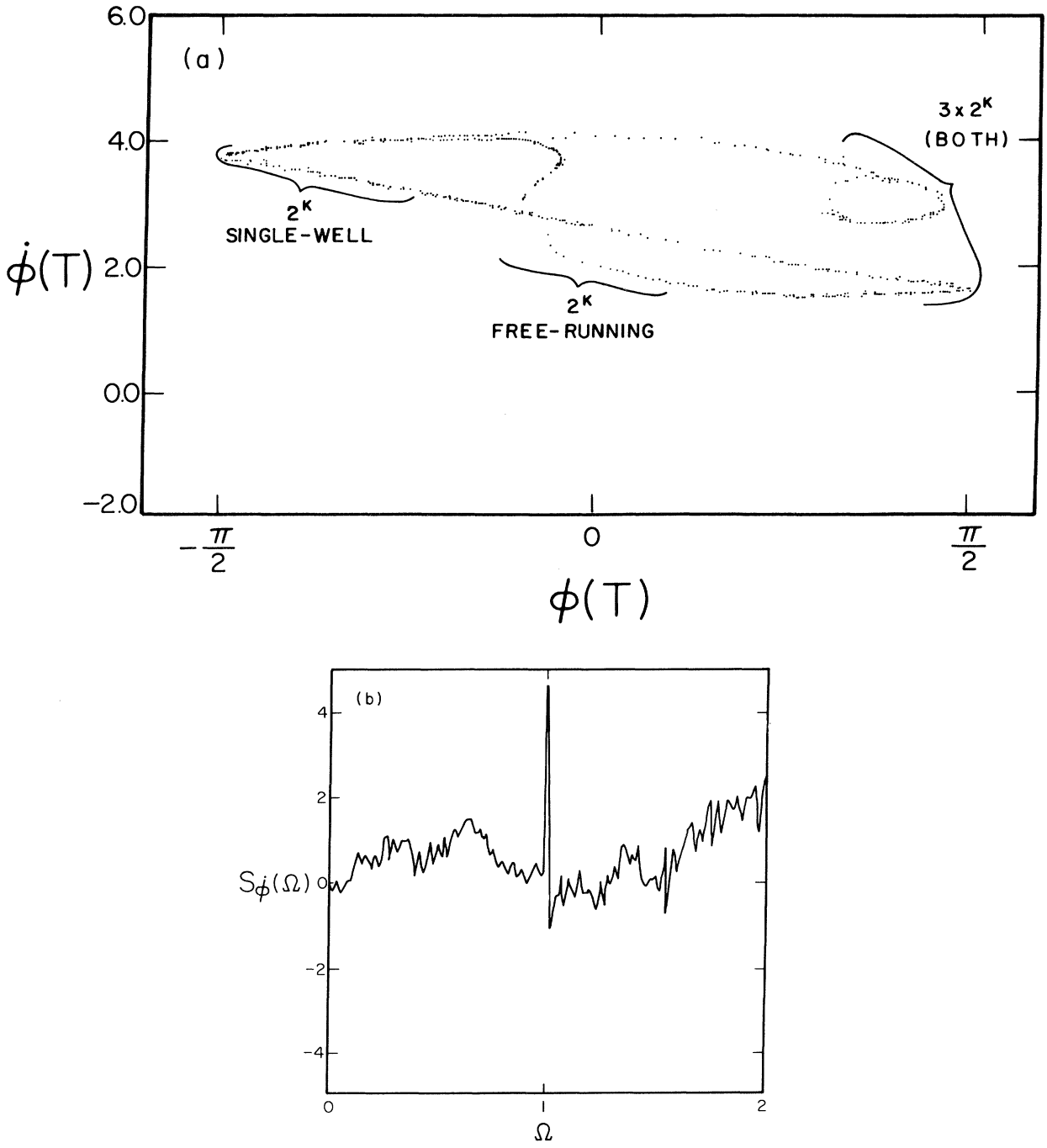

FIG. 8. (a) Poincaré map of the strange attractor corresponding to the first two regions of Fig. 1(a). The attractor is common to both regions and is a composite of the various basins of attraction, as indicated qualitatively in the figure ($\Omega=0.65$, $\beta_c=5$, $\rho=0.985$). The label indicates both that either single well or free-running solutions occur within this region. (b) Power spectrum $S_{\dot{\phi}}$ as a function of function of frequency for the strange attractor of (a).

state is characterized by a sudden chaotic (or periodic) burst as odd-period regions are approached. In the simulations it is found that while most aspects of this intermittent state agree well with the detailed analysis of Hirsh *et al.*,[22] additional features are observed. The most important difference is that the periodic laminarlike regions within the intermittent state also can exhibit sudden bursts of high-order subharmonic behavior. This is demonstrated in Fig. 12 where the voltage is shown every period as a function of time for $\rho=1.4175$ [Fig. 12(a)] and $\rho=1.419$ [Fig. 12(b)] for $\beta_c=5$ and $\Omega_{0.65}$. Note that in Fig. 12(b) the solution switches between period six and period twelve in an intermitttent fashion. In general, this phenomenon occurs only in extremely narrow amplitude windows. Careful study of similar windows of the logistic map do not show such a behavior.

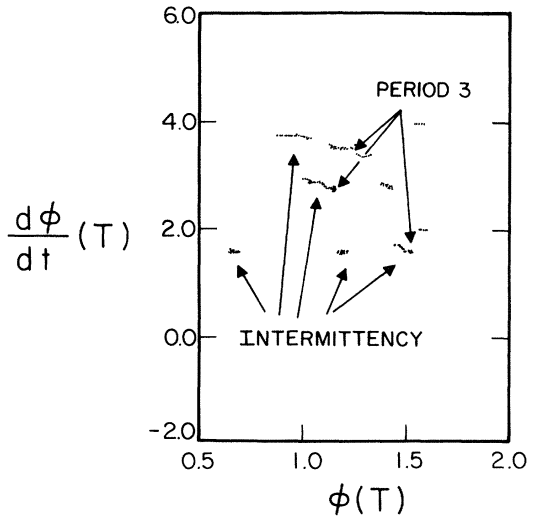

FIG. 9. Approach to a period tripling region showing the areas of the Poincaré section where intermittency takes place. The period three arrows indicate the fixed points once the period three window has reached ($\Omega=0.65$, $\beta_c=5$, $\rho=1.4175$).

VI. APPLICATIONS TO EXPERIMENTS WITH REAL JOSEPHSON JUNCTIONS

It is of interest to consider the experimental consequences of the simulations presented in this work. As expected, the optimum frequency range for observing a variety of phenomena occurs near the plasma frequency ω_p. On the other hand, the appropriate choice of β_c is not as evident. For low values of β_c ($\beta_c \leq 3$), the first transition to chaos occurs through wider amplitude ranges than at higher β_c values. However, the width in the damping plane becomes quite narrow since the minimum amplitude for observing bifurcations diverges for low β_c. This might make any experiments in this region difficult as fluctuations might switch the state of the junctions between different regions. For higher values of β_c the first transition to chaos occurs through a bifurcating region only for $\beta_c \leq 15$ and $0.6 \leq \Omega \leq 1$. However, the bifurcating region becomes narrower in amplitude as β_c is increased. Thus, $\beta_c \cong 15-10$ appears to be the optimum range for observing the initial transition to chaos. In contrast, regions higher in amplitude exhibit wider bifurcating regions preceding chaos, and more of these regions are present at higher β_c values where additional free-running solutions emerge.

The sequence of bifurcating-chaotic regions discussed in Sec. III should be readily observed, but good coupling to the radiation would be required to reach high values of the normalized amplitude ρ. This requires high-normal-state resistance junctions, which, as also discussed below, implies lower effective noise temperatures in the chaotic state.

The main experimental difficulty in the study of chaos in Josephson junctions is the detection of low-level signals at high frequencies. However, as shown in Fig. 8, the chaotic state is broadband, and thus one could characterize it by the power spectrum at frequencies well below the driving frequency. It is then interesting to define an effective noise temperature and to consider the range of effective noise temperatures predicted by simulations. The normalized power spectrum at low frequencies, $S_{\dot{\phi}}(\Omega \to 0)$, can then be related to the real voltage power spectrum

$$S_{\dot{\phi}}(\Omega \to 0) = \left[\frac{2eC}{\hbar I_c}\right]^{1/2} \frac{2e}{\hbar} S_V(\Omega \to 0) \, . \tag{7}$$

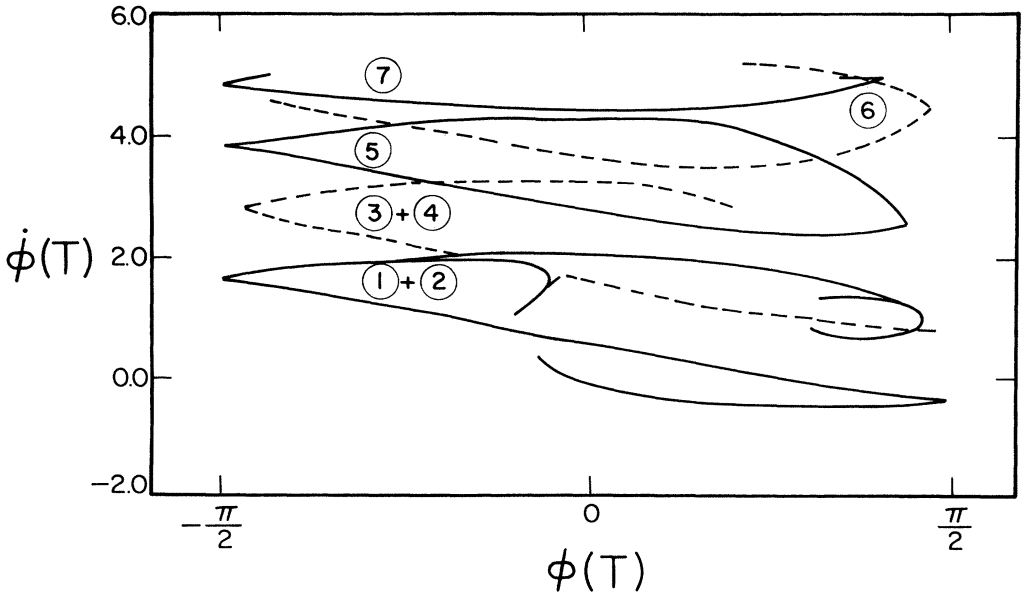

FIG. 10. Poincaré sections for the first seven regions of Fig. 1(a) showing the structure of the strange attractors. The points in the attractors have been connected with solid and dashed lines for clarity ($\beta_c=5$, $\Omega=0.65$). The numbers indicate the regions of Fig. 1(a) to which each of the attractors is associated.

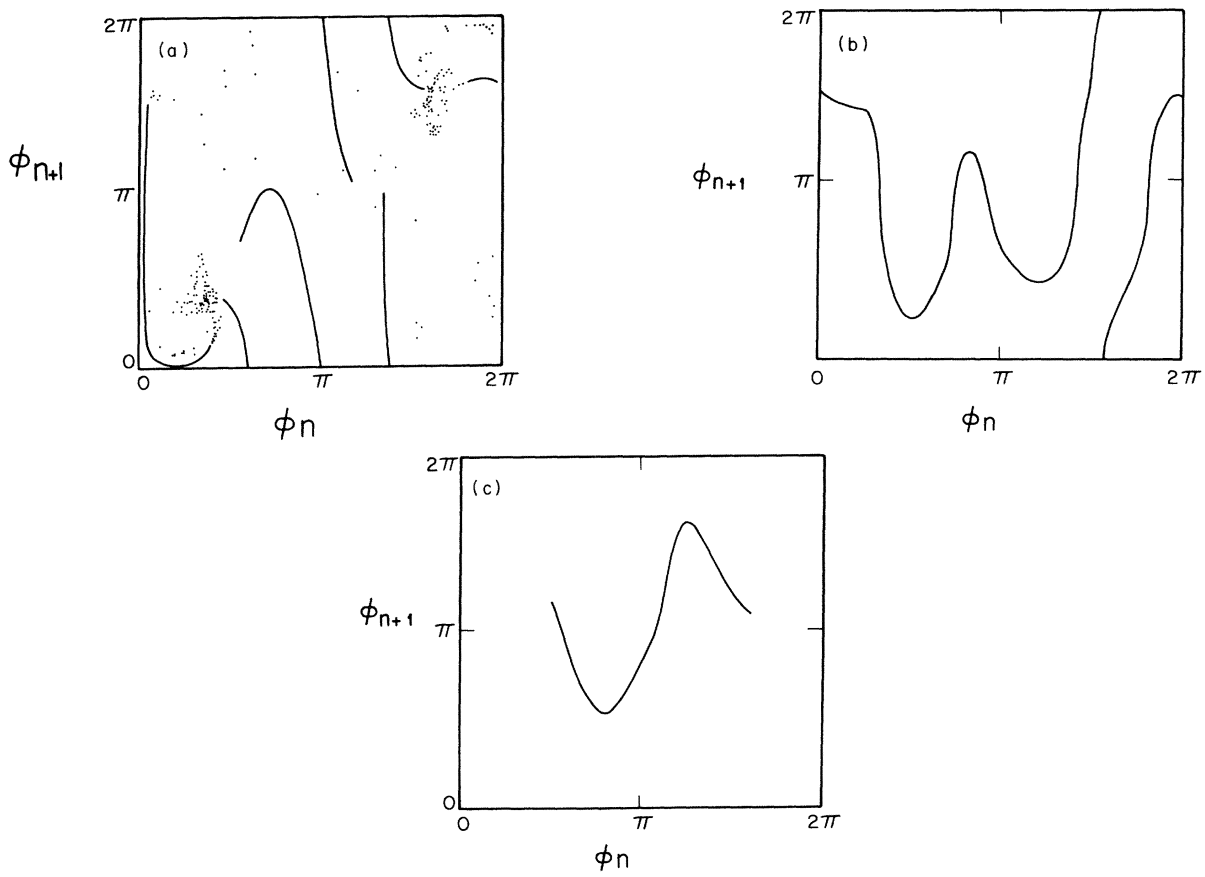

FIG. 11. Characteristic return maps $\phi_{n+1}(T)$ vs $\phi_n(T)$ (mod 2π) for three of the attractors of Fig. 10. (a) $\rho=0.985$, (b) $\rho=4.72$, and (c) $\rho=7.785$. At high amplitudes the maps are one dimensional, whereas at lower amplitudes intermittency makes the definition of a simple map difficult ($\Omega=0.65$, $\beta_c=5$).

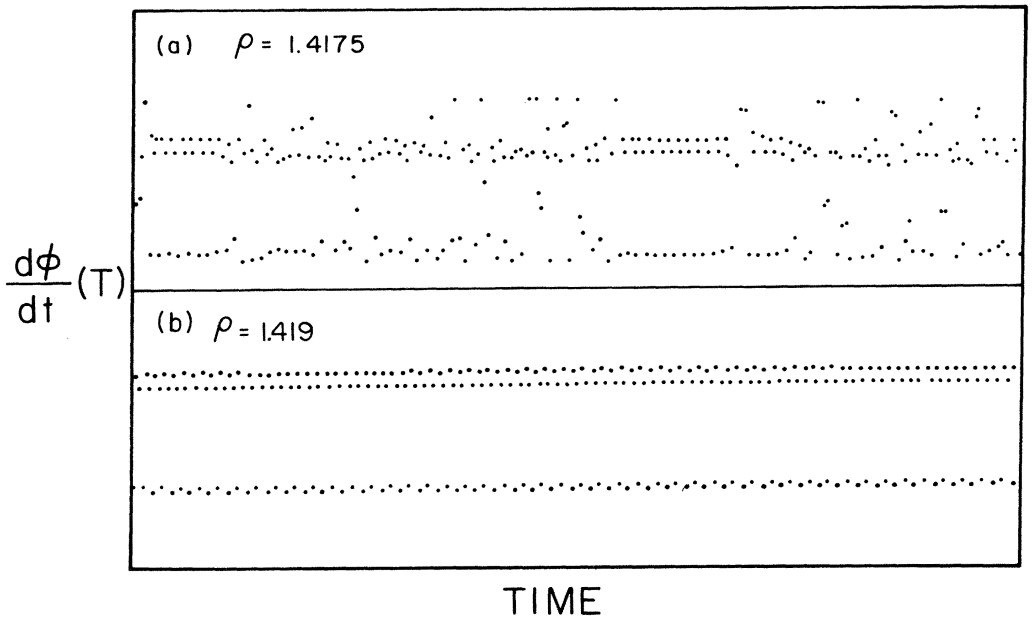

FIG. 12. $d\phi(T)/dT$ as a function of time in an intermittent region. Each point represents the value of $d\phi/dT$ for every period of the forcing frequency. Note in the lower figure how the solution switches from period three to period six.

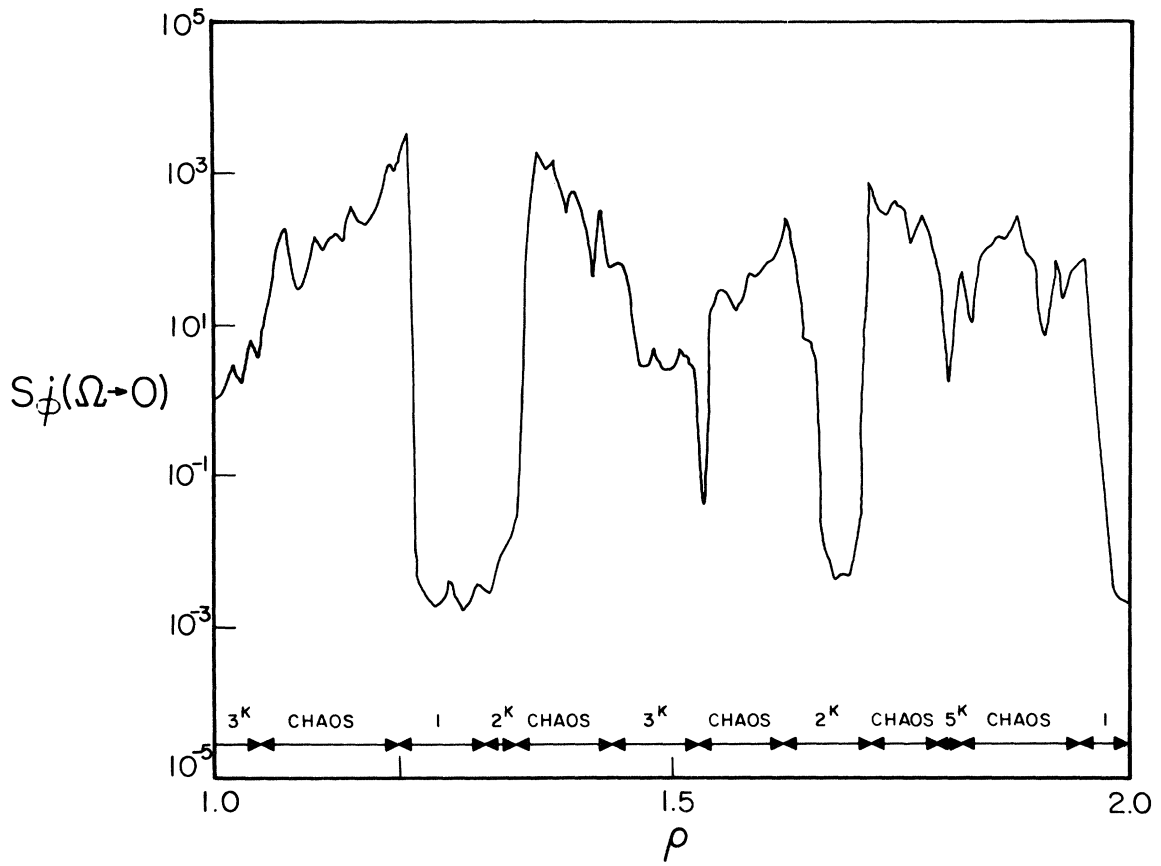

FIG. 13. Low-frequency average of the power spectrum $S_{\dot\phi}$ as a function of rf amplitude for $\beta_c=5$ and $\Omega=0.65$. The lower line indicates how the nature of the solution for each range of ρ. Note how the highest value of $S_{\dot\phi}(\Omega\to 0)$ (and thus noise temperatures) is achieved as the system leaves or approaches a chaotic region.

Assuming that an effective equivalent noise temperature $T_{\rm eff}$ can be defined by relating the calculated $S_{\dot\phi}$ to the Johnson noise value $S_V=4k_BT_{\rm eff}R_N$ per unit bandwith, then $S_{\dot\phi}=(8/\gamma)\sqrt{\beta_c}$ or

$$T_{\rm eff}=S_{\dot\phi}\frac{\hbar}{8ek_B}\frac{I_C}{\sqrt{\beta_c}}\ . \tag{8}$$

If we take as a standard a junction with a 1-mA critical current and $I_cR_N\cong 1$ mV, $\beta_c=5$ ($C\cong 0.1$ pF), then $T_{\rm eff}\sim 2.66\times 10^3 S_{\dot\phi}$ K. Figure 13 shows $S_{\dot\phi}(\Omega\to 0)$ as a function of ρ for $\beta_c=5$, simulating an experimental noise temperature of 10 K. $S_{\dot\phi}(\Omega\to 0)$ varies within the chaotic state from 1 to 10^3, corresponding to effective noise temperatures between roughly 3×10^3 and 3×10^6 K. In all the simulations performed we do not observe $S_{\dot\phi}(\Omega\to 0)$ values higher than 5×10^3. This implies an upper bound of approximately 10^6 K for our reference junction.

Note in Eq. (8) that the highest noise temperatures should occur for low-β_c, high-I_c junctions. For typical junction parameters, $T_{\rm eff}$ should have a maximum of 10^6-10^7 K. To observe the sequence of chaotic regions described in this paper, it would be necessary to use high R_N junctions; since I_cR_n is a constant Eq. (8), $T_{\rm eff}$ should be reduced in such an experiment. It is also interesting that the highest observed noise temperatures occur near transitions to and from the periodic state. In the simulations, additional noise has little impact on the chaotic temperature for the range of parameters considered.

VII. CONCLUSIONS

This paper presents extensive numerical simulations of the rf-biased Josephson junction, which show a rich variety of phenomena as the various parameters of the space of variables of the problem are changed. The most surprising feature of our simulations is that as the rf amplitude is increased a sequence of regions with bifurcating-chaotic solutions is found. Each region varies in detail from the others, but the general behavior is qualitatively similar. It has been demonstrated that further investigation of intermittency between phase-locked states is required. This phenomenon does not occur at high amplitudes where it is possible to calculate a well-behaved return map.

It has also been shown in the limit of high damping that chaotic motion does not occur below a value close to the hysteretic parameter in the I-V characteristics of

Stewart and McCumber. On the other hand, bifurcating or symmetry-breaking phenomena occur at much lower values of β_c. Free-running solutions occur only when the symmetry breaking is strong, a feature dependent, in a complex manner, on the various junction control parameters.

Finally, simulated noise temperatures indicate that experimental noise temperatures should be between 10^3 and 10^6 K, the latter being close to an upper limit for common junction parameters. It is hoped that in the near future experiments should clarify whether the same complexity observed in simulated is also observed in real Josephson junction of charge-density-wave systems. Perhaps these studies will also teach us about the limitations of the models commonly used in describing these systems.

ACKNOWLEDGMENTS

The author would like to thank J. Fernández and M. Tinkham for their encouragement. Useful discussions with G. Mata and C. J. Lobb are also gratefully acknowledged. This work was supported in part by the Venezuelan Consejo Nacional de Investigaciones Científicas y Tecnológicas (CONICIT) and the U.S. Navy Office of Naval Research. A substantial award by the Polar Foundation is also gratefully acknowledged.

[1]See, for example, J. P. Eckmann, Rev. Mod. Phys. 55, 643 (1981); E. Ott, *ibid.* 55, 655 (1981).

[2]A. H. McDonald and M. Plischke, Phys. Rev. B 27, 201 (1983).

[3]B. A. Huberman, J. P. Crutchfield, and N. H. Packard, Appl. Phys. Lett. 37, 750 (1980).

[4]R. Y. Chiao, M. J. Feldman, D. W. Peterson, B. A. Tucker, and M. T. Levinson, in *Future Trends in Superconductive Electronics,* edited by B.S. Deaver, C. M. Falco, J. H. Harris, and S. A. Wolf (AIP, New York, 1978), p. 259.

[5]D. W. Peterson, Ph.D. thesis, University of California, Berkeley, 1978.

[6]S. Wahlsten, S. Rudner, and T. Claeson, J. Appl. Phys. 854 (1978).

[7]R. L. Kautz, J. Appl. Phys. 52, 6241 (1981).

[8]R. L. Kautz, IEEE Trans. MAG-19, 465 (1983).

[9]M. J. Feigenbaum, J. Stat. Phys. 19, 25 (1978).

[10]N. F. Pederson and A. Davidson, Appl. Phys. Lett. 39, 830 (1981).

[11]D. D'Humieres, M. R. Beasley, B. A. Huberman, and A. Libchaber, Phys. Rev. A 26, 3483 (1982).

[12]W. J. Yeh and Y. H. Kao, Appl. Phys. Lett. 42, 299 (1983).

[13]E. Ben-Jacob, I. Goldhirsh, and Y. Imry, Phys. Rev. Lett. 49, 1599 (1982).

[14]R. F. Miracky, J. Clarke, and R. H. Koch, Phys. Rev. Lett. 50, 856 (1983).

[15]M. T. Levinsen, J. Appl. Phys. 53, 4294 (1982).

[16]W. C. Stewart, Appl. Phys. Lett. 12, 277 (1968); D. E. McCumber, J. Appl. Phys. 39, 3113 (1968).

[17]V. Ambegaokar and B. I. Halperin, Phys. Rev. Lett. 22, 1364 (1969).

[18]M. Cirillo and N. F. Pedersen, Phys. Lett. 90A, 150 (1982).

[19]M. J. Feldman and M. T. Levinsen, IEEE Trans. MAG-17, 834 (1981).

[20]W. J. Skocpol, M. R. Beasley, and M. Tinkham, J. Appl. Phys. 45, 4054 (1974); M. Octavio, W. S. Skocpol, and M. Tinkham, IEEE Trans. MAG-13, 739 (1977).

[21]P. Manneville and Y. Pomeau, Phys. Lett. 75A, 1 (1979).

[22]J. E. Hirsh, B. A. Huberman, and D. J. Scalapino, Phys. Rev. A 25, 519 (1982).